Comprehensive Kubo-Greenwood modelling of FDSOI MOS devices down to deep cryogenic temperatures

F. Serra Di Santa Maria, L. Contamin, M. Cassé, Christoforos Theodorou, Francis Balestra, Gérard Ghibaudo

Comprehensive Kubo-Greenwood modelling of FDSOI MOS devices down to deep cryogenic temperatures

F. Serra di Santa Maria[1], L. Contamin[2], M. Cassé[2], C. Theodorou[1], F. Balestra[1], G. Ghibaudo[1]

[1] IMEP-LAHC, Univ. Grenoble Alpes, Minatec, 38016 Grenoble, France,

[2] CEA-LETI, Univ. Grenoble Alpes, Minatec, 38054 Grenoble, France.

Email: francesco.serra-di-santa-maria@grenoble-inp.fr, gerard.ghibaudo@grenoble-inp.fr.

Abstract

A comprehensive Kubo-Greenwood modelling of FDSOI MOS devices is performed down to deep cryogenic temperatures. It is found that a single set of mobility parameters is only necessary to fit the capacitance and drain current transfer characteristics versus temperature for long channel devices. In contrast, in short channel transistors, the neutral scattering mobility component μ_N is found to decrease at small gate length due to the increased impact of neutral defects close to source/drain ends whatever the temperature. Moreover, a closed-form analytical expression for the Coulomb scattering has been developed, useful for device compact modelling.

Keywords: Kubo-Greenwood, mobility, modeling, MOSFET, FDSOI, cryogenic temperature.

1. Introduction

The Cryogenic electronics is still a key research topic as permitting circuit performance improvements in terms of operation speed, turn-on behavior, thermal noise reduction, punch-through current decrease etc. [1-5]. It finds application in high speed computing, sensing and detection, space electronics and more recently in readout CMOS electronics for quantum computing [6,7]. In this framework, the characterization and modelling of MOSFETs down to cryogenic temperatures is still a key challenge. Moreover, Kubo-Greenwood formalism has been employed as a powerful tool for the modelling of transport in MOS inversion layers, enabling detailed mobility calculations [8-10] and recently subthreshold slope calculations [11].

In this work, we propose, for the first time, to use the Kubo-Greenwood approach for the drain current modelling as a function of gate voltage in 28nm FDSOI MOSFETs down to deep cryogenic temperatures. We first validate the single 2D subband approximation for the description of the MOS inversion charge with gate voltage down to liquid helium temperatures. Then, we show that the drain current transfer characteristics can be well modeled within the Kubo-Greenwood formalism down to very low temperatures, provided phonon, Coulomb, neutral and surface roughness scattering limited mobility laws are properly calibrated.

2. Experiments details

The measurements were completed on 28nm FDSOI MOSFETs with silicon film thickness t_{si}=7nm and buried oxide (BOX) thickness t_{box}=25nm from STMicroelectronics. NMOS transistors were processed from (100) handle substrate, with <100>-oriented channel, and a high-k/metal gate Gate-First architecture [12]. Low-V_{th} transistors were available with un-doped channel through a doped back plane (NWELL doping $N_A=10^{18}cm^{-3}$) below the BOX. Thin gate oxide (with equivalent oxide

thickness EOT=1.1nm) devices with gate length L varying from 30nm up to 10µm and with gate width W=1µm or 10µm were tested using a cryogenic probe station down to 4.2K.

The gate-to-channel capacitance characteristics $C_{gc}(V_g)$ were measured with an HP 4284 LCR meter at 1MHz frequency and 10mV AC level using the standard split C-V configuration. The drain current $I_d(V_g)$ MOSFET transfer characteristics were recorded in linear region (V_d=30-50mV) with an HP4156 parameter analyzer. All the measurements were made at zero back bias. Note that the influence of back bias on the transfer characteristics has been studied in details elsewhere [13] and goes beyond the scope of this work.

3. Kubo-Greenwood transport and FDSOI MOSFET modelling

The main equations used for the Kubo-Greenwood transport and FDSOI MOSFET modelling are reminded in the following sub-sections.

3.1. Kubo-Greenwood transport modelling

The inversion layer density *n* within a single 2D subband approximation is related to the Fermi level E_f by [8,11,14],

$$n(E_f,T) = kT.A_{2d}.ln\left(1+e^{\frac{E_f-E_c}{kT}}\right) \quad (1)$$

where $A_{2D}=g.m_d^*/(\pi.\hbar)$ is the 2D density of states with g the subband degeneracy factor, m_d^* the DOS effective mass and ħ the reduced Planck constant and *kT* is the thermal energy, *T* being the temperature. Note that E_f is referred to the subband edge E_c, stated here to zero.

The inversion layer sheet conductivity, σ, which is a function of Fermi level and temperature, can be computed by integration over energy *E* of the so-called energy conductivity function $\sigma_E(E)$ as [8,11,14],

$$\sigma(E_f,T) = \int_0^{+\infty} \sigma_E(E)\left(-\frac{\partial f}{\partial E}\right)dE \quad (2)$$

where $f = 1/\left(1 + e^{\frac{E-E_f}{kT}}\right)$ is the Fermi function and,

$$\sigma_E(E) = q.E.A_{2d}.\mu(E) \tag{3}$$

with *E* being the carrier kinetic energy and *μ(E)* the energy mobility function.

When several scattering take place in the electronic transport, the energy mobility function *μ(E)* can be evaluated by the Matthiessen rule after adding the various scattering rates for each energy such as,

$$\mu(E) = \left(\frac{1}{\mu_{ph}} + \frac{1}{\mu_N} + \frac{1}{\mu_C} + \frac{1}{\mu_{SR}}\right)^{-1} \tag{4}$$

which accounts for the phonon (μ_{ph}), neutral (μ_N), Coulomb (μ_C) and surface roughness (μ_{SR}) limited mobility components, respectively.

Based on Monte Carlo quasi 2D simulations, the phonon limited mobility in an inversion layer has been established being essentially a function of temperature and vertical electric field as [15],

$$\mu_{ph}(T,F) = 1180.\left[\left(\frac{T}{300}\right)^{2.11} + \left(\frac{T}{300}\right)^{1.7}.\left(\frac{F}{F_0}\right)^{\alpha(T)}\right]^{-1} \quad (\text{cm}^2/\text{Vs}) \tag{5}$$

with *F* being the effective electric field (defined below), $\alpha(T) = 0.2.\left(\frac{300}{T}\right)^{0.1}$ and $F_0 = 7 \times 10^4$ $(\frac{V}{cm})$ a critical field.

The Coulomb scattering limited mobility is proportional to the carrier kinetic energy *E* and takes the form [8,16],

$$\mu_C(E) = 1341.\left(\frac{E}{E_{coul}}\right) \quad (\text{cm}^2/\text{Vs}) \tag{6}$$

with here E_{coul}=0.026eV. Note that $\mu_C(E_{coul})$ stands for the Coulomb mobility value at T=300K.

At this stage, it is worth noting that the Coulomb scattering energy mobility law of Eq. (6) can be used to calculate the corresponding Coulomb scattering *effective* mobility $\mu_{Ceff}=\sigma(E_f,T)/[q.n(E_f,T)]$ with the Kubo-Greenwood integral of Eq. (2) and plotted versus inversion layer density for various temperatures (see Fig. 1). As can be seen from the right figure, the Coulomb effective mobility merges the Boltzmann statistics limit at low carrier density, i.e. $\mu_{Ceff}\approx\mu_C(2kT)$, whereas μ_{Ceff} reaches the degenerate statistics asymptote at high carrier density, i.e. $\mu_{Ceff}\approx\mu_C(E_f)=\mu_C(n/A_{2d})$. As shown in Fig. 1

(dashed lines), these two asymptotic regions can be well approximated by the analytical closed-form expression,

$$\mu_{Ceff}(n,T) = \left[\mu_C(2kT)^a + \mu_C\left(\frac{n}{A_{2d}}\right)^a\right]^{\frac{1}{a}} \tag{7}$$

where the exponent a≈1.5 has been adjusted to optimize the transition between the two regions. It could be noted that Eq. (7) can be regarded as the counterpart of Eqs (5) and (8) for phonon and surface roughness scatterings.

The surface roughness limited mobility (cm^2/Vs) is mainly proportional to the square of the reciprocal effective electric field and is well approximated by the expression [17]:

$$\mu_{SR}(T,F) = \frac{8.8\times10^{14}}{F^2}.exp\left[-\left(\frac{T}{850}\right)^2\right] \qquad (cm^2/Vs). \tag{8}$$

Finally, the neutral scattering limited mobility is well known to be energy and temperature independent and simply reads [18],

$$\mu_N = Constant\ . \tag{9}$$

where the constant is proportional to the reciprocal neutral defect number.

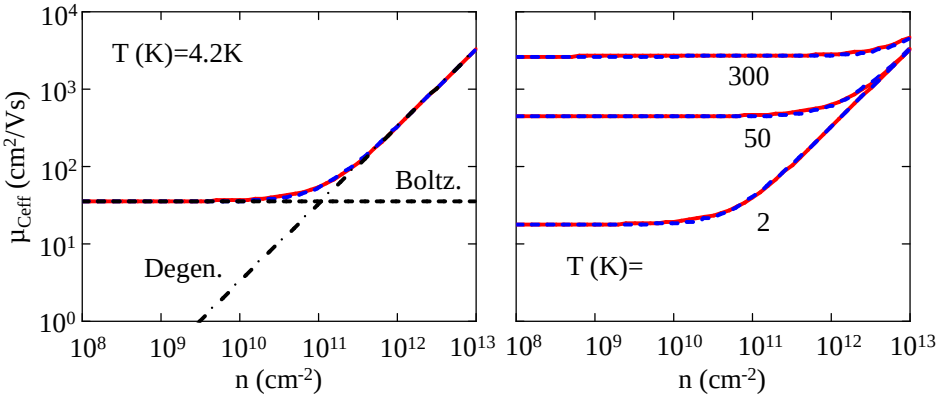

Fig. 1. Variations of Coulomb scattering effective mobility μ_{Ceff} with inversion layer density *n* for various temperatures as obtained from Kubo-Greenwood integral of Eq. (2) (red solid lines) and by analytical approximation of Eq. (7) (blue dashed lines). On the left figure are also shown the Boltzmann and degenerate statistics asymptotes.

Two options can now be used to calculate the inversion layer sheet conductivity σ as a function of inversion layer density and temperature. First, one can rigorously compute the Kubo-Greenwood integral of Eq. (2) with the energy mobility law of Eq. (4) using the Coulomb scattering energy mobility law of Eq. (6) and Eqs (5), (8)-(9) for the other scattering mechanisms. In this case, the Matthiessen rule is applied for each energy range in the integration process. Alternatively, the Kubo-Greenwood integral can be overlooked and the conductivity calculated using the explicit mobility laws versus carrier density, electric field and temperature using the Matthiessen rule applied to the mobility laws of Eqs (5), (7)-(9) and the carrier density depending on the device biasing condition (see section 3.2).

3.2 FDSOI MOSFET modelling

For the modelling of an FDSOI MOSFET device, we consider that the 2D inversion layer is located at the front oxide/silicon channel interface, such that the gate charge conservation equation reads,

$$V_g = V_{fb} + V_s + \frac{Q_i}{C_{ox}} + \frac{C_{it}.(V_s - V_0)}{C_{ox}} + \frac{C_b.(V_s - V_b)}{C_{ox}} \quad (10)$$

where $Q_i(E_f,T)=q.n(E_f,T)$ is the absolute inversion charge, V_s is the front surface potential, V_{fb} is the flat band voltage, V_g is the front gate voltage, V_b is the back bias, C_{ox} the front oxide capacitance, C_{it} ($=q.N_{it}$) is the front interface trap capacitance, N_{it} being the interface trap density, and, $C_b = (C_{si}C_{box})/(C_{si} + C_{box})$ is the substrate coupling capacitance, C_{si} being the silicon capacitance and C_{box} the BOX oxide capacitance.

The surface potential V_s can be obtained by solving Eq. (10) for given front gate voltage and back bias. Thus, the Fermi level E_f can be calculated for any bias as:

$$E_f(V_g, V_b) = q.[V_s(V_g, V_b) - V_0] \quad (11)$$

where V_0 is a reference potential depending on channel doping level.

The effective electric field F entering the phonon and surface roughness limited mobility components of Eqs (5) and (8) is evaluated by the usual expression accounting for the inversion charge and back electric field as,

$$F(V_g, V_b) = \frac{\frac{Q_i(V_g,V_b,T)}{2} + C_b.[V_s(V_g,V_b) - V_b]}{\varepsilon_{si}} \quad (12)$$

where ε_{si} is the silicon permittivity.

The drain current is then calculated in linear operation region, i.e. for small drain voltage V_d, as,

$$I_d(V_g, V_d, V_b, T, F) = \frac{W}{L}.\sigma[E_f(V_g, V_b), T, F].V_d \; . \quad (13)$$

In short channel devices, the source/drain series resistance R_{sd} effect is accounted for through Ohm's law as,

$$I_d(V_g, V_d, V_b, T, F) = \frac{\frac{W}{L}.\sigma[E_f(V_g,V_b),T,F].V_d}{1+R_{sd}.\frac{W}{L}.\sigma[E_f(V_g,V_b),T,F]} \; . \quad (14)$$

4. Results and discussion

4.1 Long channel devices

$C_{gc}(V_g)$ characteristics were measured on large area MOSFETs with W=L=10µm. The inversion charge was obtained by integration of the $C_{cg}(V_g)$ curves starting from V_g=0 as is usual in split C-V technique. Experimental and modeled $C_{gc}(V_g)$ and $Q_i(V_g)$ characteristics are shown in Fig. 2 for various temperatures. They clearly reveal the adequacy of the single subband approximation of Eq. (1) and of the MOSFET approach of Eq. (10) for the modelling of the gate charge control in FDSOI MOS transistors down to liquid helium temperature. The model parameters used in the simulation are indicated in the caption of Fig. 2.

In Fig. 3 are reported the experimental and Kubo-Greenwood modeled $I_d(V_g)$, $g_m(V_g)$ and Y-function $Y(V_g) = I_d/\sqrt{g_m}$ [19] characteristics for such a long channel device and for various temperatures, showing very good agreement. The best Kubo-Greenwood model fits have been achieved after proper calibration of the phonon, Coulomb and Surface roughness mobility law parameters, whose values are those displayed in Eqs (5), (6) and (8). It should be mentioned that these values are close to the original

ones in [8,15,17]. The value of μ_N, mentioned in Fig. 3 caption, has been set to a large value for long channel device, indicating that the neutral scattering is negligible in this case.

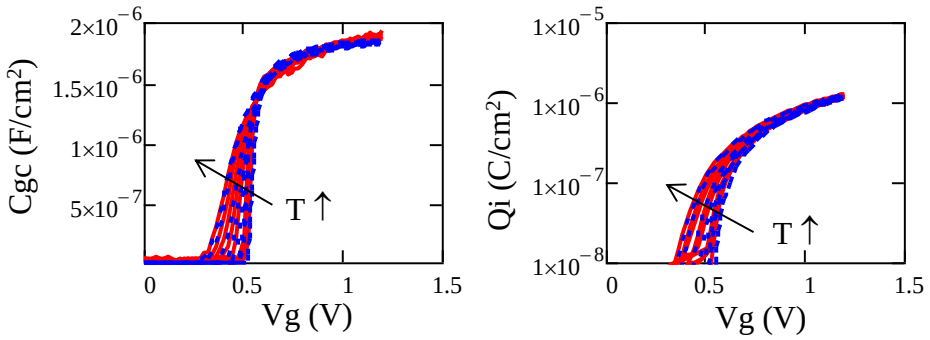

Fig. 2. Experimental (red solid lines) and modeled (blue dashed lines) $C_{gc}(V_g)$ and $Q_i(V_g)$ characteristics for various temperatures T(K)=4.2, 10, 20, 50, 100, 150, 200, 250 and 300 (W=L=10µm, model parameters: C_{ox}=2.1 µF/cm^2, C_{box}=0.14 µF/cm^2, C_{si}=1.52 µF/cm^2, C_{it}=0.16 µF/cm^2, V_0= 0.5 V).

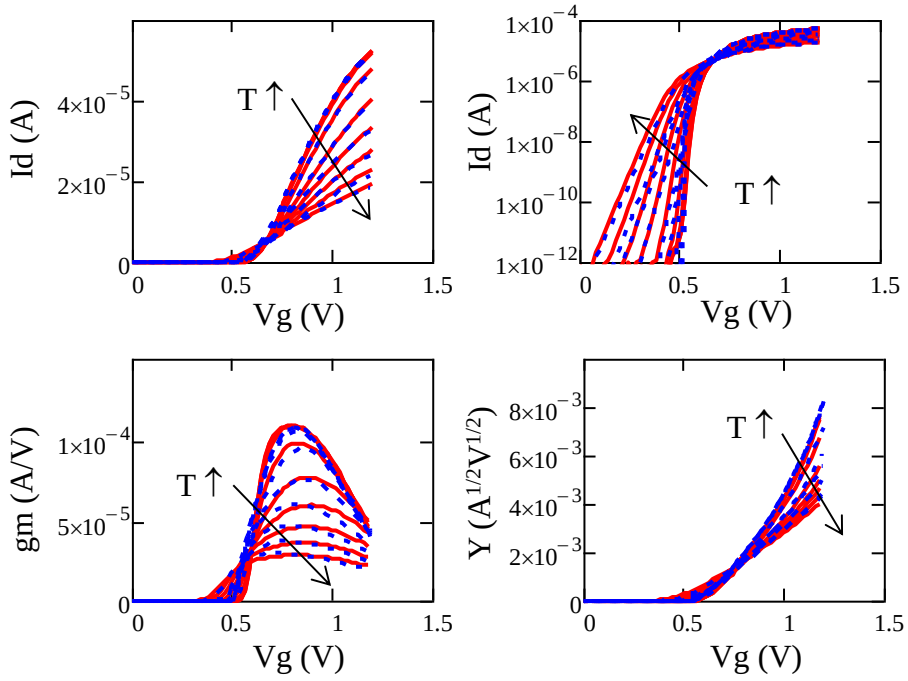

Fig. 3. Experimental (red solid lines) and modeled (blue dashed lines) I_dV_g), $g_m(V_g)$ and $Y(V_g)$ characteristics for various temperatures T(K)=4.2, 10, 20, 50, 100, 150, 200, 250 and 300 (μ_N=3000cm^2/Vs, V_d=50mV, W=L=10µm, N_{it}=2-8×10^{12}/eVcm^2).

The variations of the effective mobility, $\mu_{eff}=\sigma/(qn)$, with inversion layer density deduced from the Kubo-Greenwood modeling are shown in Fig. 4a for various temperatures. They reveal the onset of a bell-shaped mobility behavior at very low temperatures as is usual [2,8,16], due to the dominance of Coulomb and surface roughness scattering processes. Figure 4b displays the change in the temperature dependence of μ_{eff} for various carrier densities taken at weak, intermediate and strong inversion.

At low carrier density, μ_{eff} increases with temperature due to Coulomb scattering predominance (see Fig. 1) before to decrease at higher temperature due to enhanced phonon scattering. At high carrier density, μ_{eff} always decreases with temperature due to phonon diffusion supremacy. These features are also illustrated in Fig. 5, where the variations of μ_{eff} with carrier density are compared to the various mobility law components. As expected, at very low temperature, Coulomb scattering is dominating, whereas, at high temperature, phonon scattering is prevailing.

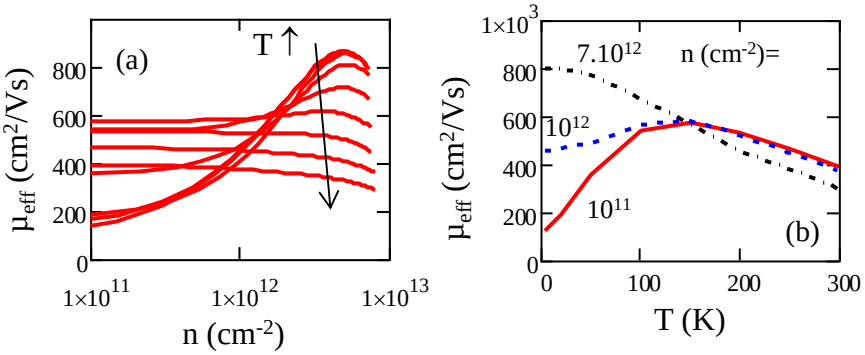

Fig. 4. a) Variations of μ_{eff} with 2D carrier density n for various temperatures T(K)=4.2, 10, 20, 50, 100, 150, 200, 250 and 300 and b) with temperature T for various 2D carrier densities as obtained from Kubo-Greenwood modeling (W=L=10µm).

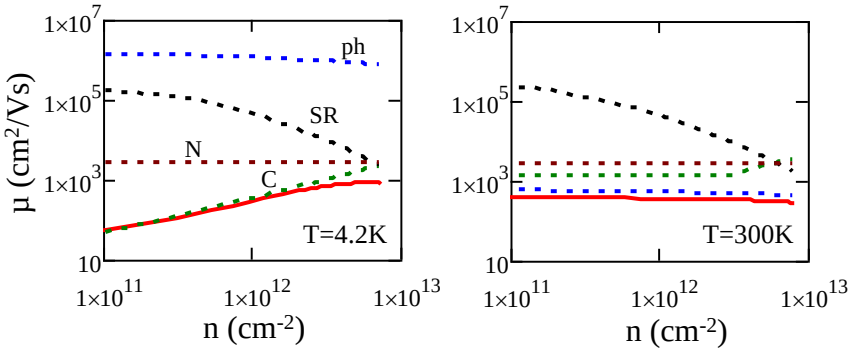

Fig. 5. Variations of μ_{eff} (red solid line) and of various scattering mobility component with 2D carrier density n for T=4.2K and T=300K as obtained from Kubo-Greenwood modeling (W=L=10μm).

In Fig. 6, we compare, for various temperatures, the variations of the effective mobility μ_{eff} with 2D carrier density as obtained from Kubo-Greenwood integral of Eq. (2) to those obtained using the Coulomb scattering mobility analytical approximation of Eq. (7). As can be seen, such an explicit analytical approximation for the Coulomb scattering mobility provides an overall good description of the global effective mobility, especially at low temperatures. For higher temperatures, a 10 to 20 % discrepancy appears at low carrier density, likely due to the error resulting from the use of the Matthiessen outside the Kubo-Greenwood integral in Eq. (2). However, the Coulomb scattering analytical mobility law of Eq. (7) could constitute a reasonably good approximation for a global effective mobility description useful for compact modelling purpose.

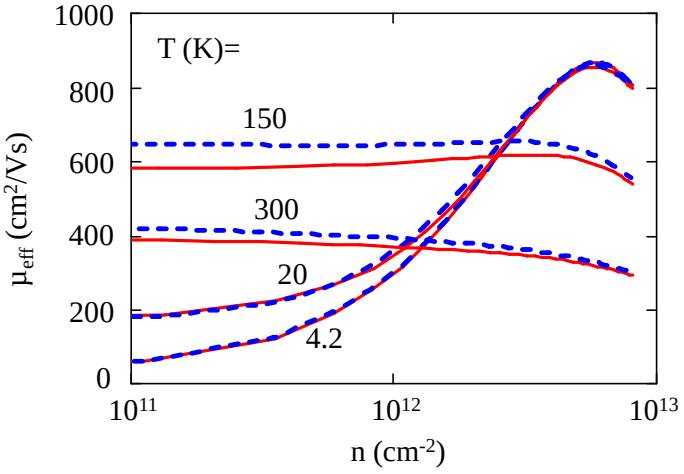

Fig. 6. Variations of μ_{eff} with 2D carrier density as obtained from Kubo-Greenwood modeling (red solid lines) and using Coulomb scattering effective mobility analytical approximation of Eq. (7) (blue dashed lines) for various temperatures (W=L=10µm).

4.2 Short channel devices

In Figures 7 and 8 are displayed the experimental and Kubo-Greenwood-modeled $I_d(V_g)$, $g_m(V_g)$ and $Y(V_g)$ characteristics for MOS devices with gate length ranging from 30nm up to 1µm and for various temperature, showing again very good agreement. In this case, it should be noted that the best Kubo-Greenwood model fits have been obtained by keeping the same mobility parameters as for long devices (Fig. 3), at the exception of the neutral mobility component μ_N, and of the reference potential V_0, which were adjusted versus gate length for each temperature as shown in Fig. 9. It is found that V_0 follows the same trend vs L as the threshold voltage exhibiting a slight roll-off due to short channel effect (not shown). However, as can be seen from Fig. 9b, μ_N is strongly degraded as the channel length is reduced, regardless of temperature, due to the increased influence of neutral defects close to source and drain in agreement with the data of [20] (square symbols in Fig. 9b) and with the theoretical analysis of [21].

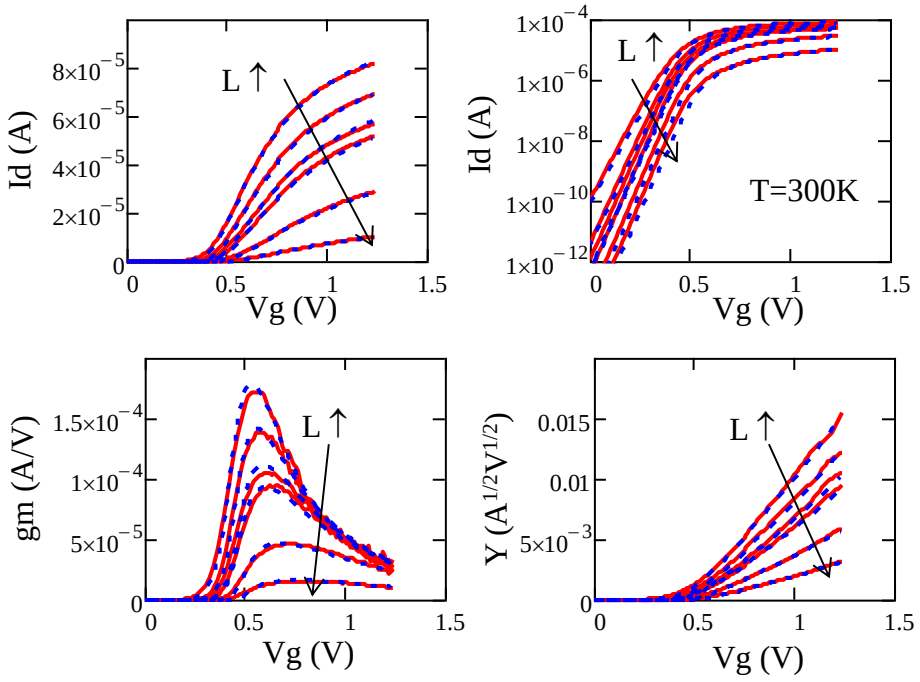

Fig. 7. Experimental (red solid lines) and modeled (blue dashed lines) I_dV_g), $g_m(V_g)$ and $Y(V_g)$ characteristics for various gate lengths L(nm)=30, 60, 90, 120, 300 and 1000 and T=300K (V_d=30mV, W=1µm).

It should also be noted that, when fitting the transfer characteristics for short channel devices, the source/drain series resistance (R_{sd}) effects were taken care using the Y-function, which is independent of R_{sd} [19]. To this end, the mobility parameter μ_N was first tuned to adjust the experimental $Y(V_g)$ curves. Then, R_{sd} was adjusted using Eq. (14) to fit the experimental $I_d(V_g)$ and $g_m(V_g)$ characteristics. Typical values for R_{sd} were found in the range 230-250Ω.µm for temperatures varying from 25K up to 300K.

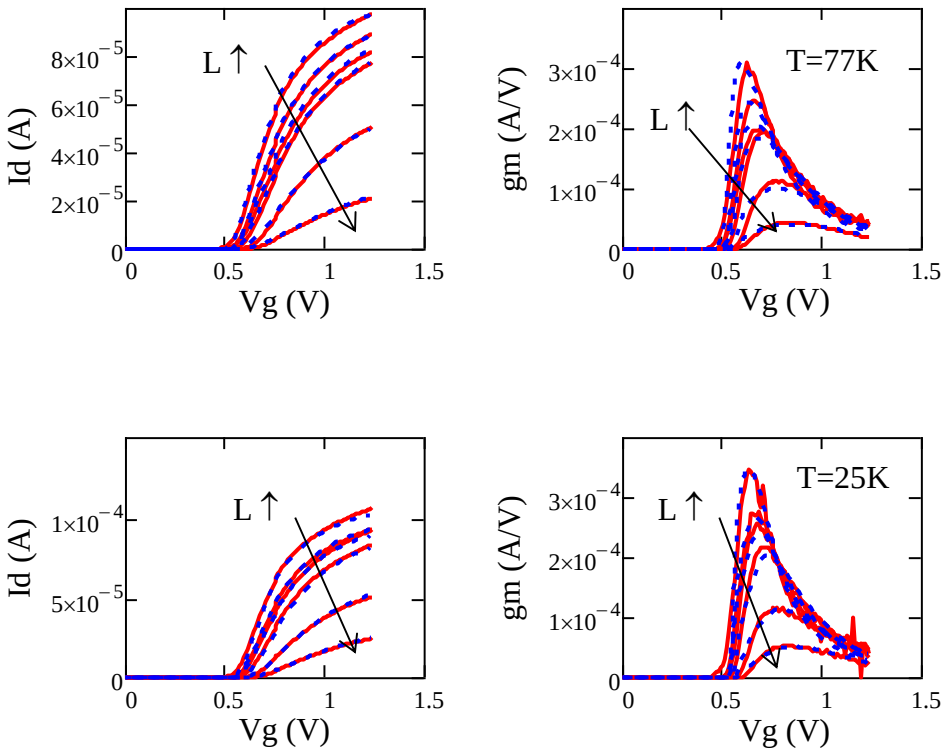

Fig. 8. Experimental (red solid lines) and modeled (blue dashed lines) I_dV_g) and $g_m(V_g)$ characteristics for various gate lengths L(nm)=30, 60, 90, 120, 300 and 1000 and for T=77K and T=25K (V_d=30mV, W=1µm).

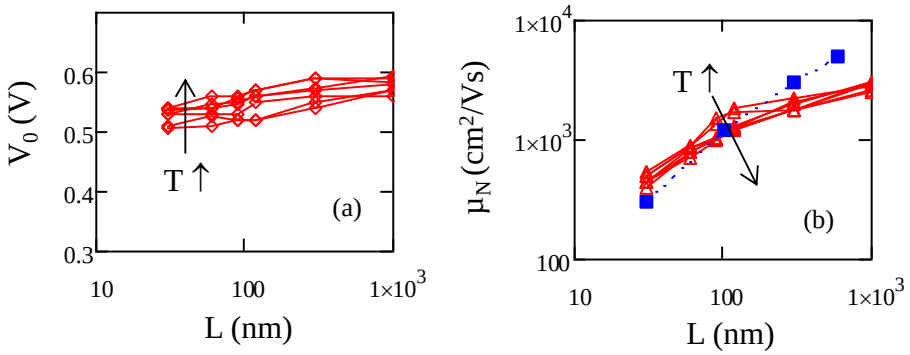

Fig. 9. Variations of (a) parameter V_0 and (b) neutral mobility component μ_N with gate length L for various temperatures T(K)= 25, 77, 100, 150, 200, 250 and 300 as obtained from Kubo-Greenwood modeling (W=1µm). The blue square symbols are results taken from [20].

5. Conclusions

A comprehensive Kubo-Greenwood modelling of FDSOI MOS devices has been performed down to deep cryogenic temperatures. Interestingly, a single set of mobility parameters was only needed to fit the data versus temperature for long channel devices. Instead, in short channel MOSFETs, the neutral scattering mobility component μ_N was found to be nearly temperature independent and to significantly decrease at small gate length due to the enhanced influence of neutral defects close to source/drain ends. Therefore, such a Kubo-Greenwood modelling can provide a physical insight into the scattering processes limiting the transport in FDSOI MOSFETs down to very low temperatures. Besides, a closed-form expression for the Coulomb scattering mobility law as a function of temperature and 2D carrier density has been established and could be very useful for the development of compact models at cryogenic temperature.

6. Acknowledgment

The authors are grateful to EU H2020 RIA project SEQUENCE (Grant No. 871764) and to ERC Synergy QuCube (Grant No. 810504) for financial support.

References

[1] E. A. Gutiérrez, J. Deen, and C. Claeys, Low temperature electronics: physics, devices, circuits, and applications. Academic Press, 2000.

[2] F. Balestra and G. Ghibaudo, Device and Circuit Cryogenic Operation for Low Temperature Electronics. Springer, 2001.

[3] T. Wada, H. Nagata, H. Ikeda, Y. Arai, M. Ohno and K. Nagase, Development of Low Power Cryogenic Readout Integrated Circuits Using Fully-Depleted-Silicon-on-Insulator CMOS Technology for Far-Infrared Image Sensors, J. Low Temp. Phys., 167, 602 (2012).

[4] R. M. Incandela, L. Song, H. Homulle, E. Charbon, A. Vladimirescu, F. Sebastiano, Characterization and Compact Modeling of Nanometer CMOS Transistors at Deep-Cryogenic Temperatures, IEEE Journal of the Electron Devices Society, 6, 996 (2018).

[5] A. Beckers, F. Jazaeri, C. Enz, Characterization and Modeling of 28-nm Bulk CMOS Technology Down to 4.2 K, IEEE J. Electron Devices Soc., 6, 1007 (2018).

[6] J.M. Hornibrook, J. I. Colless, I. D. Conway Lamb, S. J. Pauka, H. Lu, A. C. Gossard, J. D. Watson, G. C. Gardner, S. Fallahi, M. J. Manfra, and D. J. Reilly, Cryogenic control architecture for large-scale quantum computing, Phys. Rev. Applied, 3, 024010 (2015).

[7] R. Maurand, X. Jehl, D. Kotekar-Patil, A. Corna, H. Bohuslavskyi, R. Laviéville, L. Hutin, S. Barraud, M. Vinet, M. Sanquer and S. De Franceschi, A CMOS silicon spin qubit, Nature Commun., 7, 13575 (2016).

[8] G. Ghibaudo, Transport in the inversion layer of a MOS transistor. Use of Kubo-Greenwood formalism, Journal Phys. C: Solid State Physics, 19, 767 (1985).

[9] J. Dura, F. Triozon, S. Barraud, D. Munteanu, S. Martinie, and J. L. Autran, Kubo-Greenwood approach for the calculation of mobility in gate-all-around nanowire metal-oxide-semiconductor field-effect transistors including screened remote Coulomb scattering—Comparison with experiment, Journal of App. Physics, 111, 103710 (2012).

[10] O. Bonno, S. Barraud, D. Mariolle, and F. Andrieu, Effect of strain on the electron effective mobility in biaxially strained silicon inversion layers: An experimental and theoretical analysis via atomic force microscopy measurements and Kubo-Greenwood mobility calculations, Journal of App. Physics, 103, 063715 (2008).

[11] G. Ghibaudo, M. Aouad, M. Casse, S. Martinie, F. Balestra, On the modelling of temperature dependence of subthreshold swing in MOSFETs down to cryogenic temperature, Solid-State Electronics, 170, 107820 (2020).

[12] N. Planes et al., 28nm FDSOI technology platform for high-speed low-voltage digital applications, in Symposium on VLSI Technology, Digest of Technical Papers, 33, pp. 133–134 (2012).

[13] B. Cardoso Paz, et al, Front and back channels coupling and transport on 28 nm FD-SOI MOSFETs down to liquid-He temperature, Solid-State Electronics, 186, 108071 (2021).

[14] N. F Mott and E. A Davis, Electronic Processes In Non-crystalline Materials (Oxford, Clarendon, 1979).

[15] F. Gámiz and J. A. López-Villanueva, A comparison of models for phonon scattering in silicon inversion layers, Journal of Appl. Phys., 77, 4128, 1995.

[16] F. Stern, Calculated Temperature Dependence of Mobility in Silicon Inversion Layers, Phys. Rev. Lett., 44, 1469 (1980).

[17] S. Villa, A.L. Lacaita, L.M. Perron, R. Bez, A physically-based model of the effective mobility in heavily-doped n-MOSFETs, IEEE Trans Electron Devices, 45, 110 (1998).

[18] C. Erginsoy, Neutral impurity scattering in semiconductors, Phys. Rev., 79, 1013 (1950).

[19] G. Ghibaudo, A new method for the extraction of MOSFET parameters, Electronics Letters, 24, 543 (1988).

[20] M. Shin, M. Mouis, A. Cros, E. Josse, G.-T. Kim and G. Ghibaudo**,** Low temperature characterization of mobility in 14nm FD-SOI CMOS devices under interface coupling conditions, Solid State Electronics, 108, 30 (2015).

[21] G. Ghibaudo, Mobility characterization in advanced FD-SOI CMOS devices (part III pages 307-322) in "Semiconductor-On-Insulator Materials for NanoElectonics Applications", Springer, Berlin (2010).